Benzodifuran and benzodithiophene donor–acceptor polymers for bulk heterojunction solar cells

ARTICLE · FEBRUARY 2015

DOI: 10.1039/C5TA00936G

11 AUTHORS, INCLUDING:

Samodha S. Gunathilake

University of Texas at Dallas

7 PUBLICATIONS **25** CITATIONS

SEE PROFILE

John Winter Murphy

Lawrence Livermore National Laboratory

15 PUBLICATIONS **324** CITATIONS

SEE PROFILE

Weihua Hsu

Samsung

768 PUBLICATIONS **20,492** CITATIONS

SEE PROFILE

Mihaela C Stefan

University of Texas at Dallas

92 PUBLICATIONS **2,749** CITATIONS

SEE PROFILE

Journal of Materials Chemistry A

PAPER

View Article Online
View Journal | View Issue

Cite this: J. Mater. Chem. A, 2015, 3, 6980

Benzodifuran and benzodithiophene donor–acceptor polymers for bulk heterojunction solar cells†

Peishen Huang,[a] Jia Du,[a] Samodha S. Gunathilake,[a] Elizabeth A. Rainbolt,[a] John W. Murphy,[b] Kevin T. Black,[a] Diego Barrera,[bc] Julia W. P. Hsu,[b] Bruce E. Gnade,[b] Mihaela C. Stefan*[a] and Michael C. Biewer*[a]

Received 4th February 2015
Accepted 12th February 2015

DOI: 10.1039/c5ta00936g

www.rsc.org/MaterialsA

Four new donor–acceptor copolymers were synthesized by using benzo[1,2-*b*:4,5-*b*′]dithiophene and benzo[1,2-*b*:4,5-*b*′]difuran as donors and thieno[3,4-*b*]thiophene was used as the acceptor building block. A systematic study was performed to determine the influence of the combinations of different heteroatoms in the donor–acceptor copolymer. In bulk heterojunction solar cells, the polymer with all furan building blocks in the electron donating units, poly[(4,8-bis(5-dodecyl-2-furanyl)benzo[1,2-*b*:4,5-*b*′]difuran-2-yl)-*alt*-(2-ethyl-1-(3-fluorothieno[3,4-*b*]thiophen-2-yl)-1-hexanone)] (**P4**) (M_n = 66.7 kDa), achieved the highest power conversion efficiency of 5.23%.

Introduction

Furan and thiophene heterocycles are widely used as building blocks for semiconducting polymers.[1] Regioregular poly(3-hexylthiophene) (P3HT)[2,3] for example, has been extensively used in organic photovoltaics and field-effect transistors.[4] The P3HT electron donating polymer gave up to 5% power conversion efficiencies (PCE) in bulk heterojunction (BHJ) solar cells with [6,6]-phenyl-C_{61}-butyric acid methyl ester ($PC_{61}BM$) acceptor.[5–7] Being triggered by the promising performance of P3HT in organic photovoltaics (OPV), diblock copolymers[4,8] and polymer–nanoparticle hybrids[9,10] were further investigated. The relationship between the performance of solar cells and the molecular orbital energy levels of both polymer and $PC_{61}BM$ are now well established.[11,12] However, the band gap around 2 eV for P3HT limits the sunlight absorption and the conversion of the photons with longer wavelength in the photovoltaic applications.[13,14] To broaden the intrinsic absorption and adjust the HOMO/LUMO levels of the p-type semiconducting polymers, donor–acceptor (D–A) alternating copolymers were designed, synthesized, and used as donor polymers in BHJ.[15–17]

The polymers containing benzo[1,2-*b*:4,5-*b*′]dithiophene (BDT) electron donating unit in the backbone have shown promising performance in BHJ solar cells.[18,19] In BDT monomers, alkyl or alkoxyl side chains can be directly attached on the benzene core to improve the solubility of the synthesized polymers.[20,21] The commercially available polymer PTB7 with 2-ethylhexyl side chains gave a high power conversion efficiency (PCE) of 7.4% with $PC_{71}BM$ acceptor.[22,23] The effect of the different alkyl and alkoxy substituents was studied in terms of the active layer film morphologies and device PCEs.[20] The electron withdrawing carboxylate substituent was recently attached on BDT and its D–A copolymers gave PCE of ~3% with V_{oc} of 0.51 V.[24] The sp^2 hybridized carbons were also attached on the BDT to generate monomers with π-conjugation perpendicular to the polymer backbones. Benzene, thiophene, selenophene, and furan were employed as substituents on BDT.[25–28] The BDT building block was further tuned and optimized by attaching larger aromatic substituents such as thieno[3,2-*b*]-thiophene,[29] 3,3′,5-trimethyl-2,2′-bithiophene,[30,31] phenylethynyl,[32–35] and 2,2′-(5-ethylhexyl)-thienylenevinylenethiophene.[36] PCEs ranging from 1 to 8% were measured for these polymers.

Incorporation of furan, especially in 2-D conjugated structures, is relatively less developed.[37] Furan is an abundant product from renewable resources. The vegetable waste in agriculture and food industry can be converted to furfural (furan-2-carboxaldehyde),[1] while metal catalyzed decarbonylation reactions further convert furfural to furan in large scale.[38] By replacing the sulfur atoms with oxygen, the synthesis of benzo[1,2-*b*:4,5-*b*′]difuran (BDF) was straight forward.[39] Moreover, the replacement of sulfur with oxygen atoms could introduce some advantages to the photovoltaic performances of the D–A copolymers with BDF.[1] Furan building blocks with smaller atomic size of oxygen generate less steric hindrance to the

[a]Department of Chemistry, University of Texas at Dallas, 800 West Campbell Road, Richardson, TX 75080, USA. E-mail: mihaela@utdallas.edu; biewerm@utdallas.edu
[b]Department of Materials Science and Engineering, University of Texas at Dallas, 800 West Campbell Road, Richardson, Texas 75080, USA
[c]Centro de Investigación en Materiales Avanzados, S.C. (CIMAV), Unidad Monterrey, Alianza Norte 202, 66600 Apodaca, Nuevo Leon, Mexico

† Electronic supplementary information (ESI) available: Synthetic details, ^1H and ^{13}C NMR spectra of monomers and polymers, TGA and DSC curves, calculations and statistics of OPV and SCLC measurements. See DOI: 10.1039/c5ta00936g

neighboring units as compared to thiophene.[40,41] As a result, BDF polymers are expected to show smaller π–π stacking distance with more planar backbones and increased conjugation length. The relatively high electronegativity of oxygen in furan could influence the energy levels of the orbitals involved in the extended π-conjugated structures differently than sulfur. This allows for the BDF polymers to adjust the HOMO, LUMO, and band gap to further improve the optoelectronic properties. In addition, π-conjugated compounds containing furan building blocks showed improved solubility in organic solvents.[40,42] The PCEs of BDF polymers were initially below 1%.[43] In our previous work, BDF homopolymers were synthesized and studied and a phenylethynyl substituted BDF homopolymer gave PCEs of ~1.2%.[39]

More recently, BDF D–A copolymers were reported. BDF with 2-ethylhexyloxy side chains were the most studied. PCEs achieved with these polymers ranged between 4.4 and 5.2% in 2012.[44,45] Recently, 2-ethylhexyloxy substituted BDF was copolymerized with thieno[3,4-*c*]pyrrole-4,6-dione acceptors and achieved PCEs above 7%.[46] Thiophene and furan were used to extend the π-conjugation of the side chains instead of the ethylhexyloxy. BDF polymers with thiophene side chains offered PCEs above 6%,[47,48] while BDF polymers with furan side chains gave a PCE of 2.6%.[37]

In this paper, we report the synthesis and optoelectronic properties of four BDF/BDT D–A copolymers containing both furan and thiophene substituents. The studies were focused on the effects of furan building blocks in both BDF/BDT cores and side chains. Thieno[3,4-*b*]thiophene was used as the electron accepting units based on its wide study and its good performance in BDT/BDF D–A copolymers.[49,50] All four D–A copolymers were synthesized and characterized under comparable conditions.

Results and discussion

Materials design and synthesis

Four electron donating monomers with different combination of furan and thiophene building blocks were designed and synthesized as shown in Scheme 1. In our design, dodecyl side chains were attached to generate soluble polymers. Extended π-conjugation was obtained by adding furan or thiophene substituents on the BDF and BDT cores. The different chemical shifts of the aromatic protons and carbons of BDT (**M1** and **M2**) and BDF (**M3** and **M4**) monomers (Fig. 1 and S14†) are due to different π electron densities by the incorporation of different heteroatoms. Different π electron distributions in monomers indicate tuneable electronic properties in the resulting D–A copolymers. The coupling constants of protons H_a and H_b in BDT (5.67 Hz for **M1** and 5.75 Hz for **M2**) are larger than those of BDF (2.28 Hz for **M3** and 2.25 Hz for **M4**). In the electron accepting units of the D–A copolymers, the branched acyl side chains enhanced both solubility and the stability of the materials.

Bis(trimethyltin) functionalized BDT and BDF monomers were synthesized in comparable conditions. Four different polymers **P1** (**BDT-Th**), **P2** (**BDT-F**), **P3** (**BDF-Th**), and **P4** (**BDF-F**) were synthesized by Stille-coupling polymerization with

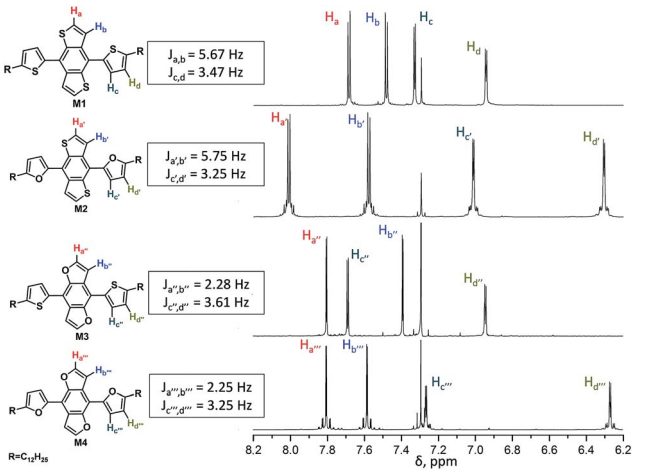

Fig. 1 Chemical shifts in ^{1}H-NMR spectra of the aromatic protons in the monomers **M1**, **M2**, **M3**, and **M4**.

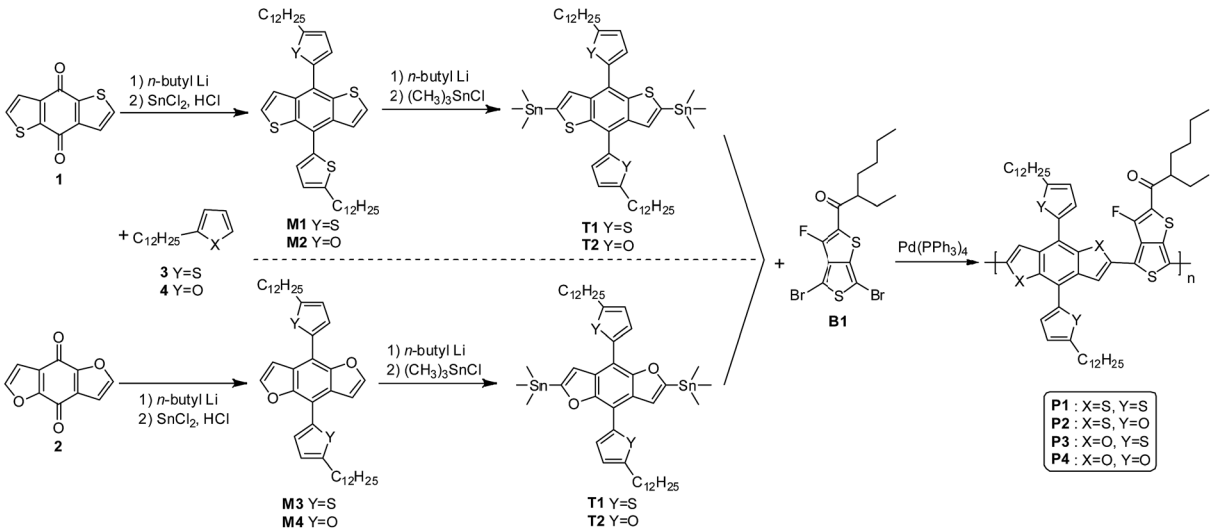

Scheme 1 Synthetic routes of BDT/BDF monomers and D–A copolymers.

tetrakis(triphenylphosphine) palladium(0) catalyst. Molecular weights of the polymers were estimated by size exclusion chromatography (SEC) with THF eluent and polystyrene calibration. The SEC data are shown in Table 1.

BDF copolymers had higher molecular weights with $M_n = 51$ kDa for polymer **P3** and $M_n = 67$ kDa for polymer **P4**. By contrast, the BDT copolymers gave lower molecular weight (Table 1 and SI†). This noticeable difference between molecular weights of BDF and BDT copolymers can be explained by the enhanced solubility brought by furan building blocks in the polymer backbones.[40,42] Stille coupling is a step growth polymerization and gave relatively broad polydispersity indexes (PDI).

The thermal stability of the synthesized D–A polymers was determined by TGA (Fig. 2). The BDT and BDF D–A copolymers showed ~5% weight loss around 400 °C. The copolymers containing furan had slightly lower decomposition temperature than the copolymer with only thiophene moieties. Amorphous nature of the copolymers was indirectly confirmed by the DSC curves (Fig. S15†) by lack of endothermic peaks. The synthesized D–A copolymers were soluble in chlorobenzene and chloroform solvents.

UV-Vis

The optical absorption spectra of the synthesized D–A copolymers were measured both on spin-coated thin film on glass substrates and in chloroform solution (Fig. 3). The copolymers displayed two absorption maxima at ~330 nm and ~700 nm (Table 2). The absorption maxima at ~330 nm are obvious longer than isolated furan (208 nm) or thiophene (215 nm and 231 nm).[51] This can be explained by π–π* transition of the 2-D

Table 1 Molecular weight and decomposition temperature of P1, P2, P3, P4

	M_n[a] (g mol^{-1})	PDI	Decomposition[b] T (°C)
P1	23 030	3.18	417
P2	33 640	2.57	400
P3	50 610	4.08	406
P4	66 700	5.06	402

[a] Estimated from SEC (THF eluent). [b] At 5% weight loss in TGA.

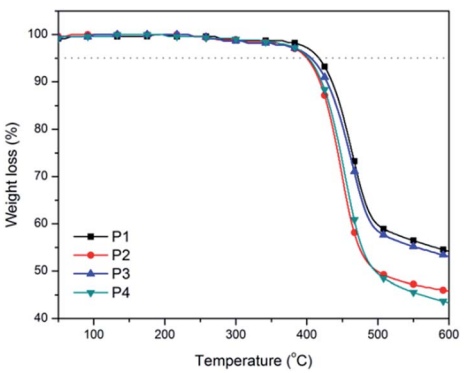

Fig. 2 TGA thermograms of P1, P2, P3, and P4.

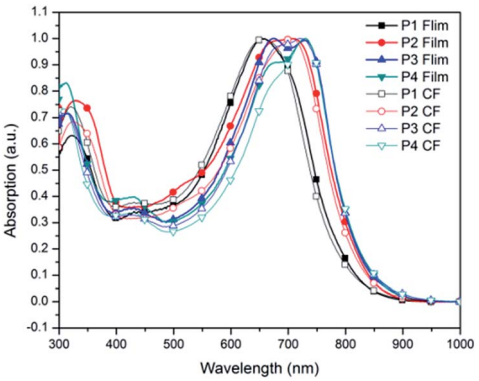

Fig. 3 UV-Vis absorption spectra of P1, P2, P3 and P4 in spin-coated thin films and in chloroform (CF).

extend π-conjugation on BDF/BDT center. The absorption band in the visible region at ~700 nm is due to the intramolecular charge-transfer transition in the D–A regions.[52] The BDT polymers, **P1** and **P2**, displayed a slight red shift in the thin film absorption spectra as compared to the chloroform solutions. This indicated the π–π stacking among the polymer backbones in the solid states.

For the **P3** and **P4**, the shoulders around 680 nm extended to the blue and displayed stronger intensities in the film absorption spectra, while the peaks at 730 nm did not change. As a result, BDF copolymers displayed broader absorption with shorter wavelength in thin film than in solution. This phenomenon is first observed among BDF D–A copolymers. A similar UV-Vis behavior can be observed in BDT D–A copolymer published by Ge's group.[48] However, the reason is not clear. The absence of strong red shifts in absorption of these four copolymers was attributed to the rigid rod conformation in both solution and solid state.

By direct measurements of UV-Vis absorption spectra of spin-coated polymer thin films on glass substrates, the attenuation coefficients (extinction coefficients), were obtained and reported (Table 2) instead of absorption coefficient in solutions.[52] In this way, the scattering and luminescence in the solid state were counted.[53] The attenuation coefficients, α, were calculated by the eqn (1), where A is absorbance, T is transmittance, z is film thickness. In order to minimize the influences of film thickness, average of 10 measurements were used (Table S1 and Fig. S16†).

$$A = -\ln T = \alpha z \quad (1)$$

At the highest absorption wavelength, the values were all above 6×10^4 cm^{-1} for the four D–A copolymers.

The absorption onset values of the D–A copolymers did not have obvious shift from the UV-Vis measurements of solutions to the thin films. Copolymer **P4** with all furan in the electron donating moiety showed the smallest $E_{g(opt)}$ of 1.50 eV. Copolymer **P1** with all thiophene had highest $E_{g(opt)}$ of 1.56 eV. The incorporation of furan in donor units (**P2–P4**) lowered the band gap by 0.04–0.06 eV compared to **P1** with all thiophene.

CV

The HOMO and LUMO levels of the polymers were estimated by CV (Fig. 4 and Table 2). For calibration, the redox potential of ferrocene/ferrocenium (Fc/Fc^+) was measured under the same conditions and located at 0.09 V *vs.* $Ag/AgNO_3$ reference electrode (Fig. S17†).[54] The value of −4.8 eV is used as absolute energy level of our electrochemical system at 0.0 V.[55] This value is also consistent with Huo *et al.*'s published data with similar CV conditions and polymer structures.[49,50] The onset values of oxidation (φ_{ox}) and reduction (φ_{re}) potentials were used to calculate the HOMO and LUMO levels of the polymers by using the following eqn (2) and (3):[56]

$$E_{HOMO}\,(eV) = -e(\varphi_{ox,Ag/Ag^+} + 4.8 - E_{1/2,Fc/Fc^+}) \quad (2)$$

$$E_{LUMO}\,(eV) = -e(\varphi_{re,Ag/Ag^+} + 4.8 - E_{1/2,Fc/Fc^+}) \quad (3)$$

The HOMO energy levels of the synthesized D–A copolymers had close values. BDT copolymer **P1** had HOMO value of −5.15 eV. The BDF copolymer **P3** and **P4** showed HOMO levels at −5.18 eV and −5.12 eV. Copolymer **P2** showed a slightly higher HOMO at −5.07 eV. For the LUMO levels, the benzodithiophene copolymers **P1** and **P2** were ~0.2 eV higher than the benzodifuran copolymers **P3** and **P4**. This suggested that the furan building blocks in the polymer backbones lowered the LUMO energy level of the materials. The extended π-conjugation generated by the furan or thiophene side chains, however, offered limited changes on the HOMO and LUMO levels of the copolymers. The copolymers with a benzodifuran core (**P3** and **P4**) had ~0.2 eV smaller electrochemical band gaps then the copolymers with a benzodithiophene core (**P1** and **P2**). The difference between optical band gap and electrochemical band gap of each copolymer is lower than 0.3 eV. This difference was shown smaller in **P3** or **P4** than **P1** or **P2**. The difference is due to the exciton binding energy.[13] Smaller variation between optical and electrochemical band gap in **P3** or **P4** implied lower binding energy of excitons in BDF copolymers than in BDT copolymers.

Photoelectron spectroscopy in air (PESA) was also used to estimate HOMO levels by measuring ionization energy of the polymers (Fig. 5).[57] The synthesized D–A copolymers had very close ionization energy around 5 eV.

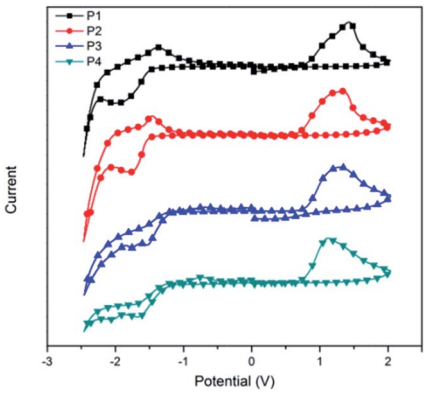

Fig. 4 Cyclic voltammograms of the **P1**, **P2**, **P3** and **P4** films on Pt electrode in 0.1 M (THP) acetonitrile solution with $Ag/AgNO_3$ reference electrode.

XRD

Thin film XRD measurements were performed on the pure polymers to investigate the influence of furan and thiophene building blocks.

Relatively broad peaks with low intensity indicated that the D–A copolymers are amorphous in the solid state (Fig. 6). The D–A copolymers displayed peaks at ~3 degrees and 24 degrees, which could be attributed to lamellar packing and π–π stacking, respectively (Table 3).[58] With the incorporation of furan to the electron donating building block, the intensity of the π–π stacking peaks increased in intensity from **P1** to **P4**. Copolymer **P4** with all furan building blocks in the electron donating units had the smallest π–π stacking distance of 3.57 Å. By contrast, copolymer **P1** with all thiophene building blocks had the largest π–π stacking distance of 3.74 Å. The XRD confirmed that smaller sized oxygen atoms can result in smaller π–π stacking distances in the solid state.

Torsional angles

Torsional angles for BDT/BDF cores with furan or thiophene substituents were calculated at the DFT B3LYP/6-31G* level of theory in the gas phase (Table 4). Only aromatic moieties were considered to simplify the calculation. Simulated ball-and-stick models are shown in Fig. 7 with both frontal and lateral views. The biggest torsional angle of 57.26° occurred with the BDT-thiophene. The combination of all thiophene building blocks

Table 2 Optical and electrochemical studies of **P1**, **P2**, **P3**, and **P4**

Polymer	HOMO[a] (eV)	HOMO[b] (eV)	LUMO[c] (eV)	$E_{g(ec)}$[d] (eV)	$E_{g(opt)}$[e] (eV)	λ_{onset}[f] (nm)	λ_{max}[f] (nm)	λ_{max}[g] (nm)	Attenuation coefficient (cm^{-1})
P1	−5.00	−5.15	−3.36	1.79	1.56	794	322, 657	321, 655	6.58×10^4
P2	−5.06	−5.07	−3.29	1.78	1.52	816	328, 708	325, 706	6.53×10^4
P3	−4.98	−5.18	−3.53	1.65	1.51	820	315, 431, 676, 728	311, 429, 682, 722	6.24×10^4
P4	−5.01	−5.12	−3.56	1.56	1.50	824	313, 431, 679, 730	309, 430, 671, 729	6.94×10^4

[a] Estimated from PESA with UV intensity of 5 nW. [b] Estimated from onset values of oxidation half cycle of CV. [c] Estimated from onset values of reduction half cycle of CV. [d] $E_g = |HOMO^b - LUMO^c|$. [e] Calculated from onset values of UV-Vis absorptions. [f] UV-Vis absorptions in spin coated thin film. [g] UV-Vis absorptions in chloroform solution.

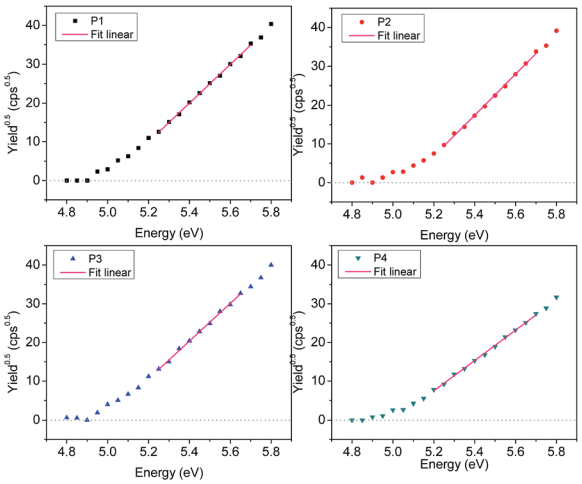

Fig. 5 The estimation of the HOMO level of **P1**, **P2**, **P3**, and **P4** by PESA with UV intensity of 5 nW.

generated very strong spatial hindrance between the core and substituents. This is mainly due to the larger atomic size of sulfur. Torsional angles decreased in both BDT-furan and BDF-thiophene (b and c in Table 4). The smaller oxygen atoms reduced the intramolecular steric hindrance. In BDF-furan, with all oxygen as the heteroatoms, the torsional angle is further reduced to only 0.1°. This small torsional angle confirms a good planar π-conjugation in BDF-furan structure and also explains the smallest *d*-spacing of π–π stacking in **P4** measured in XRD.

OPV devices and EQE

In order to keep the film thickness approximately 100 nm for the polymers with different molecular weights, different concentrations of the polymer/$PC_{71}BM$ solutions were prepared in chlorobenzene with small amount of 1,8-diiodooctane (DIO). The speed of the spin coater was kept at 1000 rpm with acceleration of 1740 rpm s^{-1}. Because the similarity of the polymer structures, **P4** was used to optimized the device fabrications

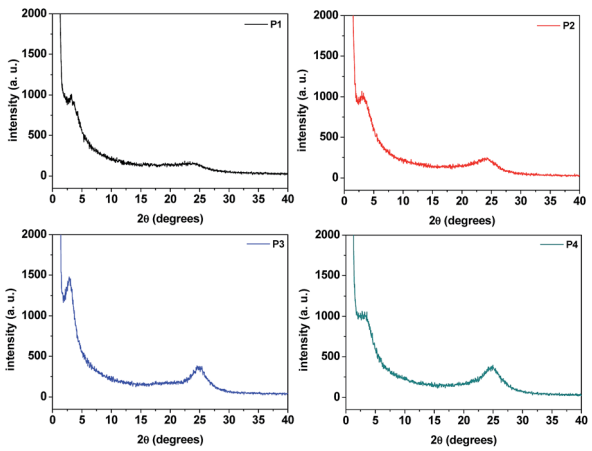

Fig. 6 XRD patterns of **P1**, **P2**, **P3**, and **P4** thin films on the SiO_2 substrates irradiated by Cu-Kα ($\lambda = 1.54$ Å) X-rays; from 1° to 40° (2θ) at 0.04° intervals, at a rate of 2 degree per min.

Table 3 XRD peak parameters for **P1**, **P2**, **P3**, **P4** in drop casted thin films

	P1		P2		P3		P4	
2θ (degrees)	3.22	23.77	3.12	24.28	2.91	24.97	3.13	24.89
d-spacing (Å)	27.42	3.74	28.30	3.66	30.34	3.56	28.21	3.57

(Fig. 8). The conditions which gave highest PCE were applied for the other polymers (Fig. 9). The ratio of polymer **P4** and $PC_{71}BM$ was the first optimized parameter (Table 5). **P4** and $PC_{71}BM$ with different weight to weight (w/w) ratios were dissolved in CB and DIO with 97/3 volume by volume (v/v). All the active layer blends were spin coated from hot solutions at 110 °C onto the hot substrates. As the data listed in the Table 5, the ratio of 1 : 1.5 offered the highest PCE.

The V_{oc} slightly increased with increasing the amount of $PC_{71}BM$, but J_{sc} decreased markedly at ratios higher than 1 : 2. The amount of DIO as the additive was then varied with fixed polymer/$PC_{71}BM$ ratio at 1 : 1.5. The J_{sc} decreased 10 times without DIO additive and was proved to be very sensitive to the amount of DIO. The results confirmed that the 3% v/v of DIO in CB gave the best device performance. With consistent 3% DIO

Table 4 Torsional angle for C_1–C_2–C_3–Y

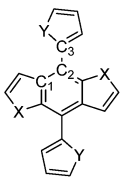

Torsional angle for C_1–C_2–C_3–Y	
(a) BDT-thiophene	57.26°
(b) BDT-furan	34.76°
(c) BDF-thiophene	30.65°
(d) BDF-furan	0.10°

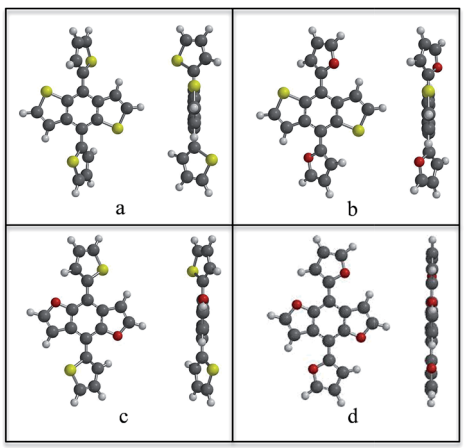

Fig. 7 All compounds calculated at the DFT B3LYP/6-31G* level of theory in the gas phase. Compounds as shown: (a) BDT with thiophene, (b) BDT with furan, (c) BDF with thiophene, (d) BDF with furan. Structures shown with BDF/BDT core in plane of page (left) and perpendicular to page (right). Yellow-sulfur, red-oxygen, gray-carbon, white-hydrogen.

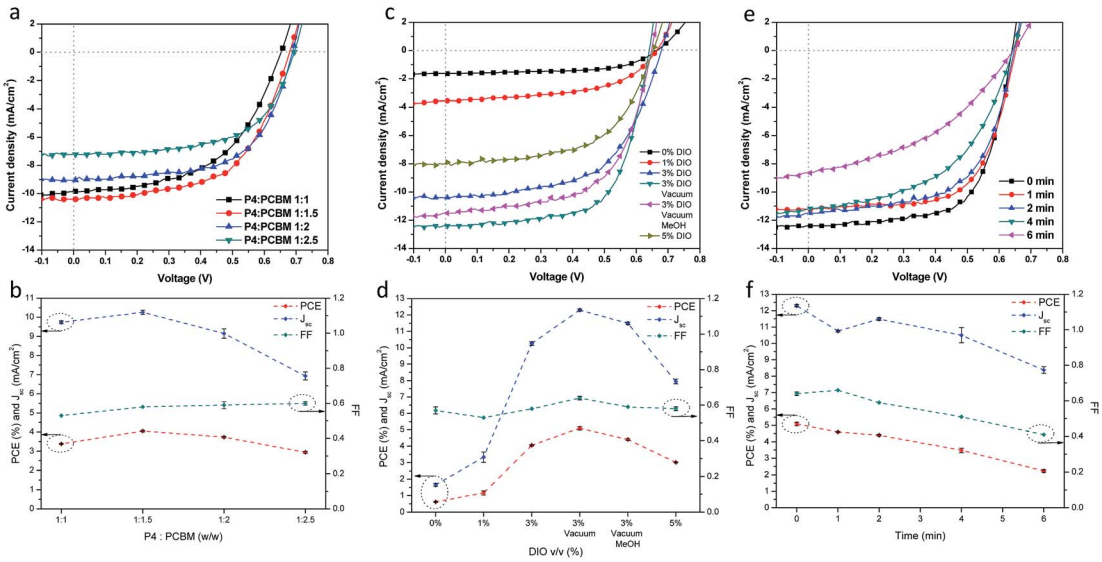

Fig. 8 *I–V* curves (top) and evolution of the merits (PCE, J_{sc} and FF) (bottom) in **P4** OPV devices with optimized (a and b) ratio between polymers and $PC_{71}BM$, (c and d) volume percentages of DIO additive, (e and f) time length of methanol treatment on the dried active layers.

and 1 : 1.5 ratio of **P4**/$PC_{71}BM$, fabrication conditions of OPV devices were optimized. Because of the high boiling point of CB, the active layers contained considerable amount of solvent, which is insulating. Thus, the devices were kept in the high vacuum chamber below 10^{-6} torr overnight to remove the residual solvent. In this way, the PCE were further increased by more than 15%. It has been reported that methanol treated surfaces of polymer/$PC_{71}BM$ blend could increase the PCE up to 30%.[59,60] However, we observed a decrease of both J_{sc} and FF with the methanol surface treatment (Fig. 8). The FF values were very sensitive and decreased dramatically for methanol treatment longer than one minute. Methanol treated active layers did not improve J_{sc} either. As a result, the best performances of **P4** was measured for the devices with polymer/$PC_{71}BM$ ratio of 1 : 1.5 in chlorobenzene with 3% v/v DIO additive under vacuum for 20 hours which gave a PCE of 5.23% (Table 6).

For **P1**, **P2**, and **P3**, the same conditions as **P4** were used for the device fabrication (Fig. 9). As shown in Table 6, copolymer **P3** gave a PCE at 3.3%, which was lower than **P4**. Copolymers **P1** and **P2** displayed similar PCEs ~2.6%. Both J_{sc} and FF increased by switching from BDT copolymers to BDF copolymers. Copolymer **P4** reached a high J_{sc} of 12.37 mA cm^{-2} and FF of 0.65. The other benzodifuran copolymer **P3** had J_{sc} of 8.05 mA cm^{-2}, which is still higher than the J_{sc} of benzodithiophene copolymers **P1** and **P2**. V_{oc} of the synthesized D–A copolymers changed in a small range of 0.1 V. This matched well with the close HOMO values of all copolymers.[61] Copolymer **P1** which had all thiophene building blocks gave a V_{oc} of 0.73 V. This value was the highest among all the synthesized D–A copolymers. Copolymer **P4** with all furan building blocks in the electron donating moieties had V_{oc} of 0.65 V. Copolymers **P2** and **P3** gave V_{oc} of ~0.68 V. Overall, the BDF copolymers performed better than the BDT copolymers.

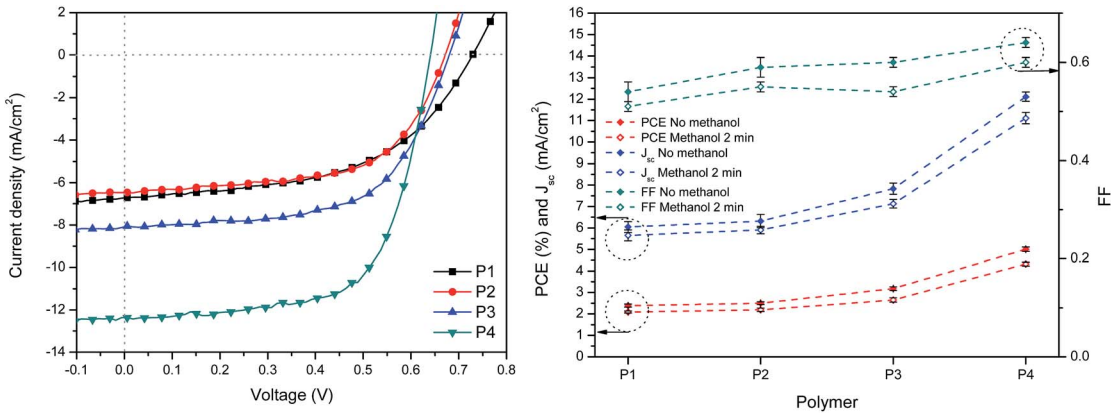

Fig. 9 *I–V* curves (left) of **P1**, **P2**, **P3**, and **P4** in OPV devices with the optimized condition (polymer/$PC_{71}BM$ ration at 1 : 1.5 w/w, 3% DIO in CB, dried under vacuum for 20 hours); and evolution of the merits (PCE, J_{sc} and FF) (right) including the effects of the methanol treatments on the dried active layers.

Table 5 OPV performances of **P4** with different device fabrication conditions

		V_{oc}[a] (V)	Avg. J_{sc} ± std[a] (mA cm^{-2})	FF[a]	Avg. PCE ± std[a] (%)	Film thickness (nm)
P4/$PC_{71}BM$[b] (w/w)	1 : 1	0.66	9.74 ± 0.07	0.53	2.39 ± 0.02	94.0
	1 : 1.5	0.68	10.26 ± 0.11	0.58	4.05 ± 0.04	96.2
	1 : 2	0.68	9.15 ± 0.25	0.59	3.73 ± 0.04	85.8
	1 : 2.5	0.67	6.93 ± 0.21	0.60	2.94 ± 0.05	85.1
DIO/CB[c] (v/v)	0%	0.66	1.66 ± 0.09	0.57	0.62 ± 0.03	92.7
	1%	0.66	3.33 ± 0.32	0.53	1.17 ± 0.21	98.5
	3%	0.68	10.26 ± 0.11	0.58	4.05 ± 0.04	96.2
	3%[d]	0.65	12.30 ± 0.07	0.64	5.09 ± 0.10	100.6
	3%[e]	0.65	11.49 ± 0.08	0.59	4.40 ± 0.05	92.1
	5%	0.66	7.94 ± 0.14	0.58	3.01 ± 0.02	96.3
Methanol treatment[f] (min)	0	0.65	12.30 ± 0.07	0.64	5.09 ± 0.10	100.6
	1	0.65	10.76 ± 0.06	0.66	4.60 ± 0.04	105.3
	2	0.65	11.49 ± 0.08	0.59	4.40 ± 0.05	92.1
	4	0.65	10.50 ± 0.46	0.51	3.48 ± 0.14	90.8
	6	0.65	8.38 ± 0.20	0.41	2.23 ± 0.07	97.6

[a] Average of 3 devices fabricated with **P4**. [b] 3% DIO in CB. [c] **P4**/$PC_{71}BM$ at 1 : 1.5. [d] Dried by high vacuum for 20 hours. [e] Dried by high vacuum for 20 hours, methanol treatment 2 min. [f] 3% DIO in CB, **P4**/$PC_{71}BM$ at 1 : 1.5, dried by high vacuum for 20 hours before methanol treatment.

External quantum efficiency (EQE) measurements were directly performed on the OPV devices. The high EQE of **P4** in the wavelength range of 300 nm to 900 nm explained its high J_{sc} in the OPV devices (Fig. 10). Copolymers **P1**, **P2**, and **P3** showed lower EQE with lower J_{sc}. Copolymer **P4** also showed the broadest EQE curve, which matched with its smallest $E_{g(opt)}$ from the UV-Vis absorption spectrum. The EQE peaks around 475 nm indicated that the $PC_{71}BM$ absorbed more photons in that range than the copolymers. The J_{sc} values estimated from EQE measurements were slightly larger than those of the OPV measurements (Table S2†). Based on the device area of 10 mm^2, the J_{sc} values reported in this work are within the discrepancy threshold and reliable.[62]

TMAFM

The surface morphology of the active layer in BHJ devices were investigated by tapping mode atomic force microscopy (TMAFM) and are shown in Fig. 11 and S18.†

The copolymer/$PC_{71}BM$ active layer blend films of the synthesized D–A copolymers showed similar phase separation textures but with different sizes of the domains. From the phase images, the granular morphologies can be observed in the films made by **P2**, while the films made by **P1** and **P3** had less obvious granular features. The height images of **P1**, **P2** and **P3** showed intense irregular height changes which indicate phase separation in large domains. Film surface of the blend with **P4** showed very small height and phase changes.

For **P1**, **P2** and **P3**, RMS values were above 4 nm. Copolymer **P2** gave a relatively rough active layer film with RMS of 6.88 nm. Copolymers **P1** and **P3** gave smoother active layer films with RMS of 4.07 nm and 3.99 nm, respectively. The RMS of **P4** was ~1.73 nm and suggested the best phase separation in the BHJ films. These results indicated that the films with smaller roughness gave better performances in the OPV devices, which is consistent with our previous finding.[30,31,33,58]

SCLC

The synthesized D–A copolymers were tested in the Schottky diode as pure polymers and polymer/$PC_{71}BM$ blends with the space charge limited current model (Table 7, Fig. 12 and ESI†).[63]

Table 6 OPV performances of **P1**, **P2**, **P3**, and **P4** with optimized device fabrication conditions

	V_{oc}[a] (V)	Avg. J_{sc} ± std[a] (mA cm^{-2})	FF[a]	Avg. PCE ± std[a] (%)	Max. PCE (%)	Film thickness[d] (nm)
P1[b]	0.73	6.04 ± 0.26	0.54	2.39 ± 0.07	2.55	87.3
P1[c]	0.72	5.65 ± 0.17	0.51	2.09 ± 0.05		
P2[b]	0.67	6.32 ± 0.31	0.59	2.50 ± 0.06	2.61	89.95
P2[c]	0.67	5.59 ± 0.17	0.55	2.19 ± 0.08		
P3[b]	0.68	7.83 ± 0.26	0.60	3.18 ± 0.09	3.34	101.6
P3[c]	0.69	7.13 ± 0.20	0.54	2.65 ± 0.10		
P4[b]	0.65	12.11 ± 0.22	0.64	5.01 ± 0.10	5.23	97.6
P4[c]	0.66	11.11 ± 0.27	0.60	4.32 ± 0.09		

[a] Average of 10 devices. [b] Device condition: (polymer/$PC_{71}BM$ ration at 1 : 1.5 w/w, 3% DIO in CB, dried under vacuum for 20 hours). [c] Same conditions with b followed by methanol surface treatment for 2 minutes. [d] Average of 10 measurements on the devices offered the maximum PCEs.

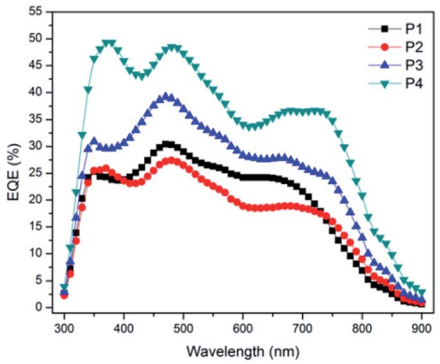

Fig. 10 EQE spectra of the polymers/$PC_{71}BM$ blends measured directly from OPV devices.

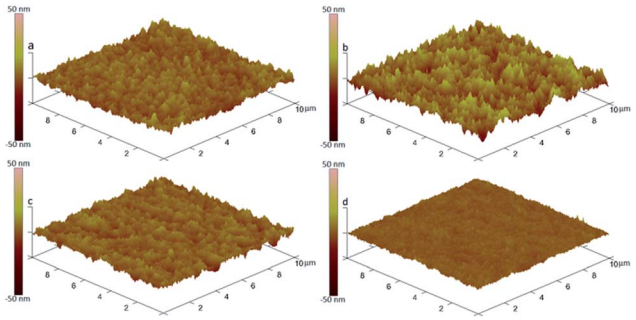

Fig. 11 3D topography of the OPV active lays with (a) **P1** (RMS = 4.07 nm), (b) **P2** (RMS = 6.88 nm), (c) **P3** (RMS = 3.99 nm), (d) **P4** (RMS = 1.73 nm)/$PC_{71}BM$ ratio 1 : 1.5 spin casted films from chlorobenzene solutions with 3% DIO followed by high vacuum for 20 hours.

Among the pure copolymers, **P3** gave the highest charge carrier mobility of 5.22×10^{-5} cm^2 V^{-1} s^{-1}. Copolymer **P4** had a charge carrier mobility of 4.61×10^{-5} cm^2 V^{-1} s^{-1}, which was larger than the BDT copolymers **P1** and **P2**. In the polymer/$PC_{71}BM$ blends, the charge carrier mobilities were higher than those of pure polymers and showed the same trend as J_{sc} values determined from the OPV devices. **P4**/$PC_{71}BM$ blend showed the highest mobility of 4.99×10^{-4} cm^2 V^{-1} s^{-1}. BDF polymers showed consistently larger charge carrier mobilities than the BDT polymers (Table 7).

Table 7 The charge mobilities in pure polymers and polymer/$PC_{71}BM$ blends

	μ^a (cm^2 V^{-1} s^{-1})	Thickness (nm)	μ^b (cm^2 V^{-1} s^{-1})	Thickness (nm)
P1	1.21×10^{-5}	73.4	7.60×10^{-5}	112.5
P2	2.48×10^{-5}	86.0	2.18×10^{-4}	117.4
P3	5.22×10^{-5}	94.3	2.38×10^{-4}	103.7
P4	4.60×10^{-5}	112.3	4.99×10^{-4}	121.8

[a] Charge mobility in pristine polymer. [b] Charge mobility in polymer/$PC_{71}BM$ blends.

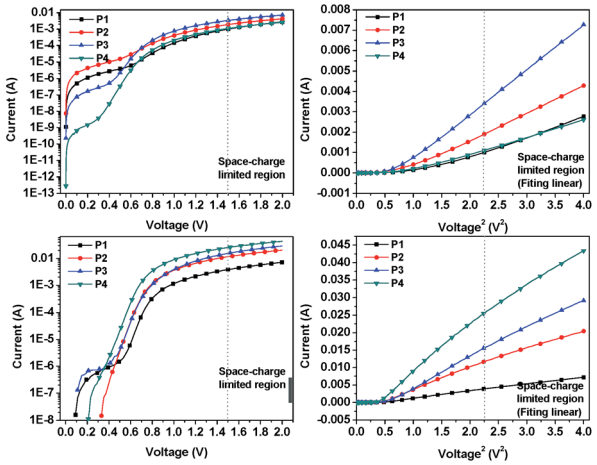

Fig. 12 I–V curves measured from pure polymers (top, left) and polymer/$PC_{71}BM$ blends (bottom, left) with the SCLC model in Schottky diodes. Fitting lines of I–V^2 curves for the calculation of the charge mobilities in pure polymers (top, right) and polymer/$PC_{71}BM$ blends (bottom, right).

Conclusions

Four BDF/BDT electron donating monomers were synthesized with different combinations of furan and thiophene building blocks. The furan and thiophene substituents offered perpendicular π-conjugation to the polymer backbones. Stille coupling polymerization was used to generate four D–A copolymers **P1**, **P2**, **P3**, and **P4**. Enhanced solubility brought by furan building blocks in polymer backbones leads to higher molecular weights of BDF copolymer **P3** and **P4** (51 and 67 kDa) than the BDT copolymers **P1** and **P2** (23 and 34 kDa). **P1** with only thiophene building blocks showed the decomposition temperature at 417 °C. The other polymers incorporated with furan had lower thermal stability at around 400 °C. All the synthesized D–A copolymers showed comparable HOMO energy level from both of the CV and PESA measurements. BDF copolymers had lower LUMO levels than the BDT polymer. This resulted in smaller band gaps for BDF polymers. In the measurements of BHJ solar cells, **P1** had the highest V_{oc} of 0.73 V, while **P4** with all furan electron donating units had the smallest V_{oc} of 0.65 V. Copolymer **P4** had the highest J_{sc} of 12.38 mA cm^{-2}. The charge mobilities of both pure polymer and polymer/$PC_{71}BM$ blend were measured in Schottky diode with SCLC model. Copolymer **P4** had the highest mobility of 4.99×10^{-4} cm^2 V^{-1} s^{-1}. This result matched with the best J_{sc} that P4 achieved in the OPV devices. A cooperative action of all the characteristics of **P4**, which contains all furan building blocks in donor, ultimately yields the best PCE of 5.23% among the four copolymers. High film quality was achieved by the high molecular weight of **P4**. At the same time, the small torsional angle of BDF-furan gathered by theoretical calculation and *d*-spacing distance of **P4** measured by XRD are among the main contributions to the good polymer/PCBM interaction and high solar cell efficiency. This result was also supported by the TMAFM study of the active layer film morphology. Overall, incorporation of furan in both

cores (**P3** + **P4** *versus* **P1** + **P2**) and in substituents (**P2** *versus* **P1**, **P4** *versus* **P3**), displayed higher PCE values compared to thiophene derivatives. This systematic study enriches the variety of the BDF family and is helpful to understand BDF building block better.

Acknowledgements

NSF (Career DMR-0956116) and Welch Foundation (AT-1740) are gratefully acknowledged for the financial support (MCS). We thank the NSF-MRI grant (CHE-1126177) for supporting the Bruker Avance III 500 NMR (MCS). DB acknowledges the support of Consejo Nacional de Ciencia y Tecnologia (CONACyT) and Project NL-2010-C33-149216, and JWPH acknowledges Texas Instruments Distinguished Chair in Nanoelectronics.

Notes and references

1 J. A. Joule and K. Mills, *Heterocyclic Chemistry*, Blackwell Publishing Ltd, 5th edn, 2010.
2 R. D. McCullough, S. Tristram-Nagle, S. P. Williams, R. D. Lowe and M. Jayaraman, *J. Am. Chem. Soc.*, 1993, **115**, 4910–4911.
3 R. D. McCullough, R. D. Lowe, M. Jayaraman and D. L. Anderson, *J. Org. Chem.*, 1993, **58**, 904–912.
4 M. P. Bhatt, H. D. Magurudeniya, E. A. Rainbolt, P. Huang, D. S. Dissanayake, M. C. Biewer and M. C. Stefan, *J. Nanosci. Nanotechnol.*, 2014, **14**, 1033–1050.
5 G. Li, V. Shrotriya, J. Huang, Y. Yao, T. Moriarty, K. Emery and Y. Yang, *Nat. Mater.*, 2005, **4**, 864–868.
6 S. Cho, K. Lee, J. Yuen, G. Wang, D. Moses, A. J. Heeger, M. Surin and R. Lazzaroni, *J. Appl. Phys.*, 2006, **100**, 114503.
7 J. M. Lobez, T. L. Andrew, V. Bulovio and T. M. Swager, *ACS Nano*, 2012, **6**, 3044–3056.
8 M. He, F. Qiu and Z. Lin, *J. Mater. Chem.*, 2011, **21**, 17039–17048.
9 K. Palaniappan, N. Hundt, P. Sista, H. Nguyen, J. Hao, M. P. Bhatt, Y.-Y. Han, E. A. Schmiedel, E. E. Sheina, M. C. Biewer and M. C. Stefan, *J. Polym. Sci., Part A: Polym. Chem.*, 2011, **49**, 1802–1808.
10 M. He, F. Qiu and Z. Lin, *J. Phys. Chem. Lett.*, 2013, **4**, 1788–1796.
11 G. Dennler, M. C. Scharber and C. J. Brabec, *Adv. Mater.*, 2009, **21**, 1323–1338.
12 A. W. Hains, Z. Liang, M. A. Woodhouse and B. A. Gregg, *Chem. Rev.*, 2010, **110**, 6689–6735.
13 S.-S. Sun and N. S. Sariciftci, *Organic Photovoltaics*, CRC Press, 2005.
14 T. M. Clarke and J. R. Durrant, *Chem. Rev.*, 2010, **110**, 6736–6767.
15 Y.-J. Cheng, S.-H. Yang and C.-S. Hsu, *Chem. Rev.*, 2009, **109**, 5868–5923.
16 H. Zhou, L. Yang and W. You, *Macromolecules*, 2012, **45**, 607–632.
17 M. He, M. Wang, C. Lin and Z. Lin, *Nanoscale*, 2014, **6**, 3984–3994.
18 M. Zhang, Y. Gu, X. Guo, F. Liu, S. Zhang, L. Huo, T. P. Russell and J. Hou, *Adv. Mater.*, 2013, **25**, 4944–4949.
19 L. Huo and J. Hou, *Polym. Chem.*, 2011, **2**, 2453–2461.
20 C. Cabanetos, A. El Labban, J. A. Bartelt, J. D. Douglas, W. R. Mateker, J. M. J. Fréchet, M. D. McGehee and P. M. Beaujuge, *J. Am. Chem. Soc.*, 2013, **135**, 4656–4659.
21 W. Li, L. Yang, J. R. Tumbleston, L. Yan, H. Ade and W. You, *Adv. Mater.*, 2014, **26**, 4456–4462.
22 J. M. Szarko, J. Guo, Y. Liang, B. Lee, B. S. Rolczynski, J. Strzalka, T. Xu, S. Loser, T. J. Marks, L. Yu and L. X. Chen, *Adv. Mater.*, 2010, **22**, 5468–5472.
23 Y. Liang, Z. Xu, J. Xia, S.-T. Tsai, Y. Wu, G. Li, C. Ray and L. Yu, *Adv. Mater.*, 2010, **22**, E135–E138.
24 K. Shibasaki, K. Tabata, Y. Yamamoto, T. Yasuda and M. Kijima, *Macromolecules*, 2014, **47**, 4987–4993.
25 S. Zhang, L. Ye, W. Zhao, D. Liu, H. Yao and J. Hou, *Macromolecules*, 2014, **47**, 4653–4659.
26 L. Ye, S. Zhang, L. Huo, M. Zhang and J. Hou, *Acc. Chem. Res.*, 2014, **47**, 1595–1603.
27 P. Sista, M. C. Biewer and M. C. Stefan, *Macromol. Rapid Commun.*, 2012, **33**, 9–20.
28 J. Warnan, C. Cabanetos, R. Bude, A. El Labban, L. Li and P. M. Beaujuge, *Chem. Mater.*, 2014, **26**, 2829–2835.
29 J.-H. Kim, C. E. Song, B. Kim, I.-N. Kang, W. S. Shin and D.-H. Hwang, *Chem. Mater.*, 2014, **26**, 1234–1242.
30 R. S. Kularatne, P. Sista, H. Q. Nguyen, M. P. Bhatt, M. C. Biewer and M. C. Stefan, *Macromolecules*, 2012, **45**, 7855–7862.
31 R. S. Kularatne, F. J. Taenzler, H. D. Magurudeniya, J. Du, J. W. Murphy, E. E. Sheina, B. E. Gnade, M. C. Biewer and M. C. Stefan, *J. Mater. Chem. A*, 2013, **1**, 15535–15543.
32 N. Hundt, K. Palaniappan, J. Servello, D. K. Dei, M. C. Stefan and M. C. Biewer, *Org. Lett.*, 2009, **11**, 4422–4425.
33 P. Sista, H. Nguyen, J. W. Murphy, J. Hao, D. K. Dei, K. Palaniappan, J. Servello, R. S. Kularatne, B. E. Gnade, B. Xue, P. C. Dastoor, M. C. Biewer and M. C. Stefan, *Macromolecules*, 2010, **43**, 8063–8070.
34 P. Sista, B. Xue, M. Wilson, N. Holmes, R. S. Kularatne, H. Nguyen, P. C. Dastoor, W. Belcher, K. Poole, B. G. Janesko, M. C. Biewer and M. C. Stefan, *Macromolecules*, 2011, **45**, 772–780.
35 P. Sista, J. Hao, S. Elkassih, E. E. Sheina, M. C. Biewer, B. G. Janesko and M. C. Stefan, *J. Polym. Sci., Part A: Polym. Chem.*, 2011, **49**, 4172–4179.
36 H.-S. Chung, W.-H. Lee, C. E. Song, Y. Shin, J. Kim, S. K. Lee, W. S. Shin, S.-J. Moon and I.-N. Kang, *Macromolecules*, 2014, **47**, 97–105.
37 Y. Zhang, L. Gao, C. He, Q. Sun and Y. Li, *Polym. Chem.*, 2013, **4**, 1474.
38 S. Sitthisa and D. E. Resasco, *Catal. Lett.*, 2011, **141**, 784–791.
39 P. Sista, P. Huang, S. S. Gunathilake, M. P. Bhatt, R. S. Kularatne, M. C. Stefan and M. C. Biewer, *J. Polym. Sci., Part A: Polym. Chem.*, 2012, **50**, 4316–4324.
40 O. Gidron, Y. Diskin-Posner and M. Bendikov, *J. Am. Chem. Soc.*, 2010, **132**, 2148–2150.
41 Y. Miyata, T. Nishinaga and K. Komatsu, *J. Org. Chem.*, 2005, **70**, 1147–1153.

42 A. T. Yiu, P. M. Beaujuge, O. P. Lee, C. H. Woo, M. F. Toney and J. M. J. Fréchet, *J. Am. Chem. Soc.*, 2012, **134**, 2180–2185.
43 H. Li, P. Tang, Y. Zhao, S.-X. Liu, Y. Aeschi, L. Deng, J. Braun, B. Zhao, Y. Liu, S. Tan, W. Meier and S. Decurtins, *J. Polym. Sci., Part A: Polym. Chem.*, 2012, **50**, 2935–2943.
44 L. Huo, Y. Huang, B. Fan, X. Guo, Y. Jing, M. Zhang, Y. Li and J. Hou, *Chem. Commun.*, 2012, **48**, 3318–3320.
45 B. Liu, X. Chen, Y. Zou, L. Xiao, X. Xu, Y. He, L. Li and Y. Li, *Macromolecules*, 2012, **45**, 6898–6905.
46 J. Warnan, C. Cabanetos, A. El Labban, M. R. Hansen, C. Tassone, M. F. Toney and P. M. Beaujuge, *Adv. Mater.*, 2014, **26**, 4357–4362.
47 B. Liu, B. Qiu, X. Chen, L. Xiao, Y. Li, Y. He, L. Jiang and Y. Zou, *Polym. Chem.*, 2014, **5**, 5002–5008.
48 Y. Wang, F. Yang, Y. Liu, R. Peng, S. Chen and Z. Ge, *Macromolecules*, 2013, **46**, 1368–1375.
49 L. Huo, S. Zhang, X. Guo, F. Xu, Y. Li and J. Hou, *Angew. Chem., Int. Ed.*, 2011, **50**, 9697–9702.
50 L. Huo, L. Ye, Y. Wu, Z. Li, X. Guo, M. Zhang, S. Zhang and J. Hou, *Macromolecules*, 2012, **45**, 6923–6929.
51 A. R. Katritzky, C. A. Ramsden, J. A. Joule and V. V. Zhdankin, *Handbook of Heterocyclic Chemistry*, Elsevier, 3rd edn, 2010.
52 P. M. Beaujuge, C. M. Amb and J. R. Reynolds, *Acc. Chem. Res.*, 2010, **43**, 1396–1407.
53 M. Nic, J. Jirat and B. Kosata, http://goldbook.iupac.org/index.html, release 2.3.3 edn, 2014.
54 Y. Zou, A. Najari, P. Berrouard, S. Beaupre, B. R. Aich, Y. Tao and M. Leclerc, *J. Am. Chem. Soc.*, 2010, **132**, 5330–5331.
55 C. M. Cardona, W. Li, A. E. Kaifer, D. Stockdale and G. C. Bazan, *Adv. Mater.*, 2011, **23**, 2367–2371.
56 Y. Li, Y. Cao, J. Gao, D. Wang, G. Yu and A. J. Heeger, *Synth. Met.*, 1999, **99**, 243–248.
57 W. R. Salaneck and M. Fahlman, *J. Mater. Res.*, 2011, **19**, 1917–1923.
58 P. Sista, B. Xue, M. Wilson, N. Holmes, R. S. Kularatne, H. Nguyen, P. C. Dastoor, W. Belcher, K. Poole, B. G. Janesko, M. C. Biewer and M. C. Stefan, *Macromolecules*, 2012, **45**, 772–780.
59 H. Zhou, Y. Zhang, J. Seifter, S. D. Collins, C. Luo, G. C. Bazan, T.-Q. Nguyen and A. J. Heeger, *Adv. Mater.*, 2013, **25**, 1646–1652.
60 Y. Wang, Y. Liu, S. Chen, R. Peng and Z. Ge, *Chem. Mater.*, 2013, **25**, 3196–3204.
61 K. Vandewal, A. Gadisa, W. D. Oosterbaan, S. Bertho, F. Banishoeib, I. Van Severen, L. Lutsen, T. J. Cleij, D. Vanderzande and J. V. Manca, *Adv. Funct. Mater.*, 2008, **18**, 2064–2070.
62 E. Zimmermann, P. Ehrenreich, T. Pfadler, J. A. Dorman, J. Weickert and L. Schmidt-Mende, *Nat. Photonics*, 2014, **8**, 669–672.
63 V. Shrotriya, Y. Yao, G. Li and Y. Yang, *Appl. Phys. Lett.*, 2006, **89**, 063505.